Revista Brasileira de Farmacognosia
April 2020, Volume 30 Issue 2 Pages 155-168
https://doi.org/10.1007/s43450-020-00036-2
https://archimer.ifremer.fr/doc/00630/74194/

Carotenoids from *Rhodomonas salina* Induce Apoptosis and Sensitize A2058 Melanoma Cells to Chemotherapy

De Oliveira-Júnior Raimundo Gonçalves [1], Nicolau Elodie [2], Bonnet Antoine [1], Prunier Grégoire [1], Beaugeard Laureen [1], Joguet Nicolas [3], Thiéry Valérie [1], Picot Laurent [1, *]

[1] Littoral Environnement et Sociétés (LIENSs, UMRi CNRS 7266), La Rochelle Université, La Rochelle, France
[2] Laboratoire Physiologie et Biotechnologie des Algues, Institut Français de Recherche pour l'Exploitation de la Mer, Nantes, France
[3] IDCAPS, R&D INNOV'IA, La Rochelle, France

* Corresponding author : Laurent Picot, email address : laurent.picot@univ-lr.fr

Abstract :

Melanoma is an aggressive tumor with invasive and metastatic potential, frequently exhibiting multidrug resistance mechanisms. In our continuous search for antimelanoma molecules, we have identified some effective marine compounds capable of not only inducing cell death, but also of sensitizing chemoresistant tumor cells to clinically used anticancer drugs. In this report, the cryptophyte Rhodomonas salina (Wislouch) D.R.A.Hill & R.Wetherbee, Pyrenomonadaceae, was chemically investigated in order to identify pigments efficiently inhibiting melanoma cells proliferation. All pharmacological tests were performed on A2058 cells expressing the oncogenic BRAF V600E mutation and resistant to dacarbazine treatment. Flash chromatography of R. salina ethanol extract led to purification of alloxanthin and crocoxanthin, which showed significant antiproliferative activity against A2058 cells, exhibiting IC50 = 29 and 50 µM, respectively. These carotenoids promoted growth inhibition, decreased cell migration, and induced apoptosis and sub-G1 cells accumulation after 72 h of treatment. In addition, alloxanthin potentiated the cytotoxic activity of vemurafenib (a BRAF inhibitor) and restored the sensitivity of A2058 cells to dacarbazine treatment.

Graphical abstract

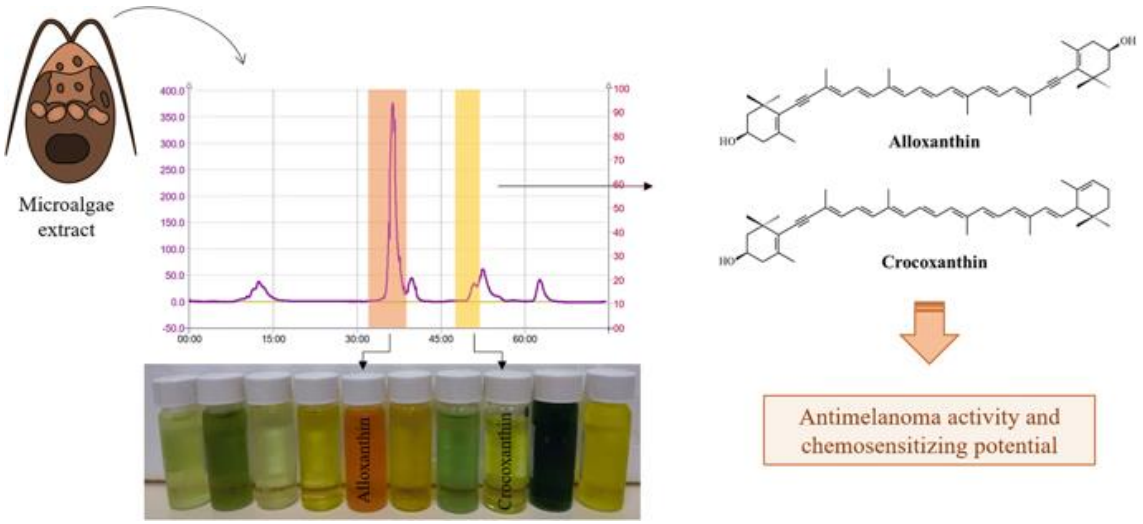

Keywords : Alloxanthin . Chemosensitivity, Crocoxanthin, Cutaneousmelanoma, Drug resistance, Microalgae

Introduction

Cutaneous melanoma is an aggressive tumor deriving from melanocyte cells. In Europe, more than 20 000 people die from melanoma every year. It is the most frequent tumor in young adults aged 25 to 35 years old, and it is responsible for 70% of mortality by skin cancers (Schadendorf et al., 2018). The incidence of melanoma is increasing worldwide and most cases are associated with excessive exposure to UV radiation. In addition, advanced and metastatic melanoma (stages III and IV) have very poor prognosis and the overall positive responses to monotherapy using conventional anticancer drugs are weak, ranging from 4 to 26% (Matthews et al., 2017; Prado et al., 2019; Tracey and Vij, 2019).

The classical antimelanoma drugs include alkylants agents (e.g. dacarbazine, temozolomide, fotemustine, carmustine, semustine), platinum drugs (cisplatin and carboplatin), vinca alkaloids (vindezine and vinblastine), taxanes (docetaxel and paclitaxel) and tamoxifen (Garbe et al., 2016). Recently, promising results have been obtained with immunotherapy (monoclonal antibodies, e.g. ipilimumab), target therapy (BRAF inhibitors, e.g. vemurafenib; MEK inhibitors, e.g. cobimetinib) and combined treatments (BRAF inhibitors associated to MEK inhibitors, e.g. vemurafenib + cobimetinib) (Napolitano et al., 2018; Schadendorf et al., 2018). However, these treatments induce severe toxicity, including neutropenia, thrombocytopenia, fatigue, nausea, vomiting, and neurosensory troubles (Jang and Atkins, 2014; Lopatka et al., 2018; Roos et al., 2014; Voskoboynik and Arkenau, 2014). The wide range of antineoplastic treatments ineffective at killing melanoma cells implies that the drug resistance mechanisms in melanoma are complex. In fact, melanoma cells are constitutively or adaptively resistant to pro-apoptotic drugs, acquiring mutations and cellular adaptations during the treatment that result in intrinsic survival mechanisms (Spagnolo et al., 2015, 2014; Tentori et al., 2013). Cytotoxic molecules usually lead to the selection of tumor cells variants overexpressing efflux transporters, such as P-glycoprotein (P-gp) and multidrug-resistance factor-1 (MDR1), and anti-apoptotic proteins (e.g. Bcl-2, Bcl-xL, Mcl-1), which justifies treatment failure (Housman et al., 2014).

Microalgae are a source of biomolecules considered not only promising dietary supplements (Gille et al., 2018), but also compounds that possess several therapeutic properties such as antioxidant, anti-inflammatory (Habashy et al., 2018), hypocholesterolemic (Sengupta et al., 2018) and anticancer (Juin et al., 2018). Among these compounds, a range of bioactive carotenoids can be isolated, including β-carotene, fucoxanthin, zeaxanthin, lutein, violaxanthin, echinenone and canthaxanthin, and some of them are produced exclusively by microalgae (Casagrande et al., 2019). These pigments have often been associated with anticancer effects,

including against cutaneous melanoma cell lines (Baudelet et al., 2013; Haguet et al., 2017; Pasquet et al., 2011). They exert antiproliferative effect by inducing apoptosis and modulating signalling pathways involved in survival, cell proliferation, invasion and metastasis. Moreover, some carotenoids have been particularly investigated in combined treatments with drugs clinically used in melanoma therapy. In a recent study, we demonstrated that zeaxanthin isolated from *Porphyridium purpureum* sensitizes chemoresistant human melanoma cells to vemurafenib, enhancing its antiproliferative effect (Juin et al., 2018). Indeed, the use of natural molecules as sensitizer agents has been encouraged because of their low *in vivo* toxicity, allowing the reduction of effective doses of conventional anticancer drugs and consequently limiting potential toxic effects without affecting the therapeutic response (de Oliveira Júnior et al., 2018; Vinod et al., 2013).

In this report, we continue our search for new antimelanoma molecules through a chemical and pharmacological investigation of *Rhodomonas salina*. It is a marine cryptophyte microalga, known to be rich in starch and routinely used in the diet of different invertebrate species (Chaloub et al., 2015; Tremblay et al., 2007). We have previously shown that chlorophyll c_2, alloxanthin and β-carotene are the most common pigments found in *R. salina*, which makes it a promising source not only of nutrients but also of bioactive compounds (Serive et al., 2017). Nevertheless, many carotenoids remain unknown in this species and their anticancer potential has not yet been properly explored. In the present study, we describe the complete pigment profile of *R. salina* extract and the antiproliferative activity of two of its most promising carotenoids (alloxanthin and crocoxanthin) against chemoresistant human melanoma cells (A2058 cells) expressing the oncogenic BRAF mutation.

Materials and Methods

Microalgae culture, harvest and freeze-drying

Rhodomonas salina CCAP 978/27 was grown in a commercial 16 L photobioreactor LUCY© (Synoxis algae, Le Cellier, France) containing 0.2 µm filtered and autoclaved seawater enriched with Walne's medium 4 $ml.L^{-1}$ (Walne, 1970). The culture was realized in batch condition with a continuous irradiance of 120 µmol $photons.m^{-2}.s^{-1}$ photosynthetically active radiation (PAR) in a climate room at 18°C. A pH 9 regulation was maintained with a regulated CO_2 injection. After 20 days, cells reached a concentration of $5.84.10^6$ $cell.ml^{-1}$. At this early stationary phase, 16 L of the culture were harvested by centrifugation. The microalgae paste

was freezed at -80°C and freeze-dried before extraction. Additional information about the microalga species is available in the supplementary material.

Sonication-assisted extraction of R. salina pigments

Pigments were extracted from the lyophilized biomass (2 g) in absolute ethanol (500 ml). The mixture was sonicated at 50 W–30 kHz (UP50H ultrasonicator, Hielscher Ultrasonics GmbH, Germany) for 30 min, on ice and under constant stirring (Haguet et al., 2017). The extractive solution was filtered (PVDF 0.22 µm membrane) and the solvent was evaporated under vacuum, resulting in the *R. salina* extract (Rs-EtOH, 0.53 g).

Scanning electron microscopy (SEM)

To confirm cell rupture during sonication-assisted extraction, *R. salina* cells were freeze-dried before or after sonication, placed on a conductive double layer carbon support and examined by SEM using a Philips-FEI Quanta 200 ESEM/ FEG microscope (environmental mode) equipped with a FEG canon delivering 1 to 30 kV beam current (Haguet et al., 2017).

UPLC-DAD-MS/MS analysis

Pigment profile of Rs-EtOH was obtained by ultra-high performance liquid chromatography system (Acquity UPLC H-class, Waters Milford USA) coupled to a photodiode array (Waters 2996) or a high resolution mass spectrometry (XEVO G2S Q-TOF) equipped with an electrospray ionization source (Waters, Manchester, England). The UPLC system was formed by a quaternary pump (Quaternary Solvent Manager, Waters) and an automatic injector (Sample Manager-FTN, Waters) equipped with a 10 µl injection loop. 10 µl (DAD analysis) or 5 µl (MS analysis) of Rs-EtOH solution were injected in a C18 column (Acquity UPLC BEH C18, Waters) (2.1 × 50 mm, 1.7 µm), using a flow rate of 300 $\mu l.min^{-1}$ and a gradient composed of solvents A (water/formic acid, 100/0.001, v:v) and B (methanol/formic acid, 100/0.001, v:v), according to the following procedure: 0–1 min, 80% B; 1–2 min, 80%–81% B; 2–5 min, 81% B; 5–7 min, 81–81,5% B; 7–10 min, 81.5% B; 10-11 min, 81.5%-83% B; 11-14 min, 83% B; 14-16 min, 83%-85% B; 16-20 min, 85% B; 20-23 min, 85%-95% B; 23-27 min, 90% B; 27-29 min, 90%-95% B; 29-35 min, 95% B; 35-37 min, 95%-98% B; 37-43 min, 98% B; 43-44 min, 100% B; 44-48 min, 100% B; 48-48.5 min, 100%-20% B; 48.5-51 min, 20% B. During the analysis, the column and the injector were maintained at 25 °C and 7 °C, respectively. The instrument was adjusted for the acquisition on a 300–800 nm interval in UV mode, with 5 $spectra.s^{-1}$ and 1.2 nm of resolution. The analyses were

performed in positive ionization mode with MSE function in a centroid mode. Final ESI conditions were: source temperature 120 °C, desolvation temperature 500 °C, gas flow-rate of the cone 50 $L.h^{-1}$, desolvation gas flow-rate 800 $L.h^{-1}$, capillary voltage 3.0 kV, sampling cone 130 V and source compensation 80 V. The instrument was set to acquire over the *m/z* 250–1300 m/z interval, with a scan time of 0.15 s. The mass spectrometer was calibrated before analysis using 0.5 mM sodium formate solution. Leucine Enkephalin (M = 555.62 Da, 1 $ng.\mu l^{-1}$) was used as a lock-mass. UPLC-DAD chromatogram was recorded at 300-800 nm (full scan) and UPLC-MS/MS data were collected in positive mode (ESI^+). The mass error between experimental and theoretical parent and fragment ions was calculated as ([experimental m/z − theoretical m/z]/ theoretical m/z) × 10^6 (ppm).

Purification of alloxanthin and crocoxanthin

Rs-EtOH was fractioned by flash liquid chromatography, using an Interchim Puriflash PF430 system. Rs-EtOH (100 mg) was solubilized in methanol and added to 10 g of celite® 545 (Sigma-Aldrich®, France). The mixture was homogenized manually until complete solvent evaporation and then placed in a pre-column. The pre-column containing Rs-EtOH-adsorbed celite® was coupled on the top of a PF-C18 column (20 g, 15 µm) and eluted with a mobile phase composed of a ternary solvent gradient: A (methanol/water, 80/20), B (acetonitrile/water, 90/10) and C (isopropanol). The gradient flow program was set as follows: 0-5 min, 100% A; 5-9 min, 100% B; 9-45 min, 30% B and 70% C; 45-50 min, 100% C; 50-55 min, 100% C; 55-60 min, 100% B; 60-65 min, 100% A; 65-70 min, 100% A. The flow rate was 5 $mL.min^{-1}$ and elution was monitored at 450 nm, with an automatic collector (10 ml per tube). This fractionation protocol was adapted from a previous study (Baudelet et al., 2013), considered an effective method for purification of microalgae pigments, especially carotenoids.

Cell viability assay

All pharmacological assays were performed using A2058 (ATCC® CRL-11147™) cell line. A2058 are highly invasive and metastatic human melanoma cells, BRAF-mutated (Ronca et al., 2013), tumorigenic at 100% frequency in nude mice (supplier's information) and very to conventional chemotherapy (de Oliveira Júnior et al., 2019). Cells were grown in DMEM (Dutscher, France), supplemented with 10% heat-inactivated (56 °C, 30 min) FCS (Dutscher, France) and penicillin-streptomycin (1000 $U.ml^{-1}$ and 100 $\mu g.ml^{-1}$, respectively) (Dutscher, France), at 37 °C in a 5% CO_2 humidified atmosphere. Rs-EtOH and isolated carotenoids were solubilized in DMSO before dilution in the cell culture medium. The DMSO final concentration

was lower than 1% and tested as negative control. A2058 cells (2 x 10^3/well) were treated with Rs-EtOH (1-100 µg.mL^{-1}), alloxanthin (1-100 µM) or crocoxanthin (1-100 µM). After 72h, cell viability was measured using the MTT assay as previously described (Juin et al., 2018; Mosmann, 1983). Cell morphology was evaluated after treatments under inverted phase contrast microscope (Nikon, Eclipse, France). IC_{50} was calculated by nonlinear regression analysis using Prism 6.0 (GraphPad Software).

Cell migration assay

Antimigratory activity of alloxanthin and crocoxanthin was determined as previously reported (Cisilotto et al., 2018). A2058 cells (2 x 10^4/well) were incubated and grown to 90% confluence in 24-well plates. Cell monolayers were scratched with a sterile plastic tip, washed with PBS and incubated in a fresh cell culture medium containing alloxanthin (14.5 µM, ½IC_{50}) or crocoxanthin (25 µM, ½IC_{50}), for 48h. Cell migration was microscopically monitored at 0, 24 and 48h (ZEISS Axion Observer, France), and results were expressed as percentage of cell migration calculated by measuring the cell surface using ImageJ® software.

Annexin V-Cy3 / 6-CFDA analysis

Cells were incubated for 24h and subsequently treated with alloxanthin (29 µM, IC_{50}) or crocoxanthin (50 µM, IC_{50}). After 72h of treatment, cells were washed with PBS and double stained with annexin V-Cy3 (red fluorescence) and 6-carboxyfluorescein diacetate (6-CFDA, green fluorescence) solution according to manufacturer's recommendations (Sigma-Aldrich®, France) and finally observed under fluorescent microscope (ZEISS Axion Observer, France) (de Oliveira Júnior et al., 2019).

Nuclear fragmentation

Cells were incubated for 24h in 4-well chamber slides (5000 cells/well) and then treated with alloxanthin (29 µM, IC_{50}) or crocoxanthin (50 µM, IC_{50}) for 72h. Cells were washed in PBS before being fixed with formaldehyde 4% solution for 30 min at 37 °C. Subsequently, cells were washed in PBS, permeabilized with Triton X-100 1% and finally stained with DAPI according to manufacturer's instructions (ProLong™ Gold Antifade Mountant with DAPI kit, ThermoFischer Scientific, France). Nuclear condensation and fragmentation of untreated and treated cells were observed under fluorescent microscope (ZEISS Axion Observer, France).

Caspase-3 activity

Caspase-3 activity was determined using a colorimetric assay (CASP3C kit, Sigma-Aldrich®, France) as previously reported. Cells were treated with alloxanthin (29 µM, IC_{50}) or crocoxanthin (50 µM, IC_{50}) for 72 h. After treatment, cells were washed with PBS, lysed with lysis buffer, and caspase-3 activity (µmol pNA/min/ml) was measured according to manufacturer's instructions.

Cell cycle analysis

A2058 cells were treated with alloxanthin (29 µM, IC_{50}) or crocoxanthin (50 µM, IC_{50}) for 72h before being stained with PBS containing propidium iodide (PI 100 $\mu g.ml^{-1}$), Rnase A (100 $\mu g.mL^{-1}$) and 0.1% Triton X-100 (ThermoFisher Scientific, France) for 15 min, at 37°C. Cells were analysed using a FACS Cantoll flux cytometer (BD Biosciences, France) equipped with an air cooled blue LASER (λ = 488 nm, 20 mW) as previously described (Juin et al., 2018).

Sensitization of A2058 cells to vemurafenib and dacarbazine

Vemurafenib (Selleckchem®, France) and dacarbazine (Sigma-Aldrich®, France) were diluted to a 10 mM stock solution in PBS, before dilution in cell culture medium. A2058 cells were treated for 72h with increasing concentrations of vemurafenib (1-100 µM) or dacarbazine (1-100 µM), alone or combined to alloxanthin (14.5 µM, ½IC_{50}) or crocoxanthin (25 µM, ½IC_{50}). Antiproliferative activity of monotherapies and combined therapies was calculated using MTT assay as described above and results were expressed as IC_{50}. The combination index (CI) was calculated using the software CompuSyn (version 1.0), according to Chou-Talalay method (Chou and Talalay, 1984). CI < 1.0 indicates synergism, CI > 1.0 indicates antagonism, and CI values equal to 1.0 indicate additive effect.

Statistical analysis

Data were expressed as mean ± SEM and analyzed by unpaired Student's *t* test or one-way ANOVA followed by Tukey's multiple comparison test (statistical significance when $p<0.05$), according to the case, using Prism 6.0 (GraphPad software). Pharmacological results were obtained from at least three independent measurements (n=3 or more).

Results and Discussion

Sonication-assisted extraction of R. salina pigments

Microalgae have hard cell wall in most of cases, which limits metabolites extraction by conventional methods. Accordingly, sonication-assisted extraction has been increasingly used to obtain compounds from different microalgae as previously demonstrated by our research group (Baudelet et al., 2013; Haguet et al., 2017; Juin et al., 2015). To ensure complete extraction of pigments, *R. salina* freeze-dried biomass was sonicated for 30 min at 50 W-30 kHz, using ethanol as solvent. Scanning electron microscopy of freeze-dried biomass before sonication revealed cells with intact cell morphology. In contrast, *R. salina* cells showed cell wall disruption after sonication-assisted extraction, allowing the direct contact of the solvent with the intracellular content (supplementary data).

Pigment profile of R. salina extract (Rs-EtOH)

UPLC-DAD-MS/MS analysis of Rs-EtOH was achieved in a single 51 min run and 18 peaks were identified according to their UV, MS and MS/MS spectral data (Fig. 1 and Table 1). Chlorophylls c_2 and *a*, pheophytin *a* and the carotenoids alloxanthin, monadoxanthin, crocoxanthin and β,ε-carotene were the main pigments identified, corroborating previous chemical investigation involving *R. salina* (Kaňa et al., 2012; Serive et al., 2017; Vu et al., 2016). Alloxanthin, monadoxanthin and crocoxanthin are carotenoids of frequent occurrence in the *Rhodomonas* genus, since they have been reported in *R. baltica*, *R. lens* and *R. minuta* (Rodriguezl, 2000; Sanz et al., 2015; Teubner et al., 2003; van Houcke et al., 2017). Chlorophyll c_2, chlorophyll *a* and pheophytin *a* derivatives (hydroxyl, methoxylactone and ethoxylactone forms) were also detected. Although these derivatives are naturally occurring in microalgae (Baudelet et al., 2013; Haguet et al., 2017; Hynninen, 1981; Juin et al., 2015), they may have originated during the extraction procedure due to the high chlorophyll instability. Chemical structures of the main identified molecules are presented in supplementary data.

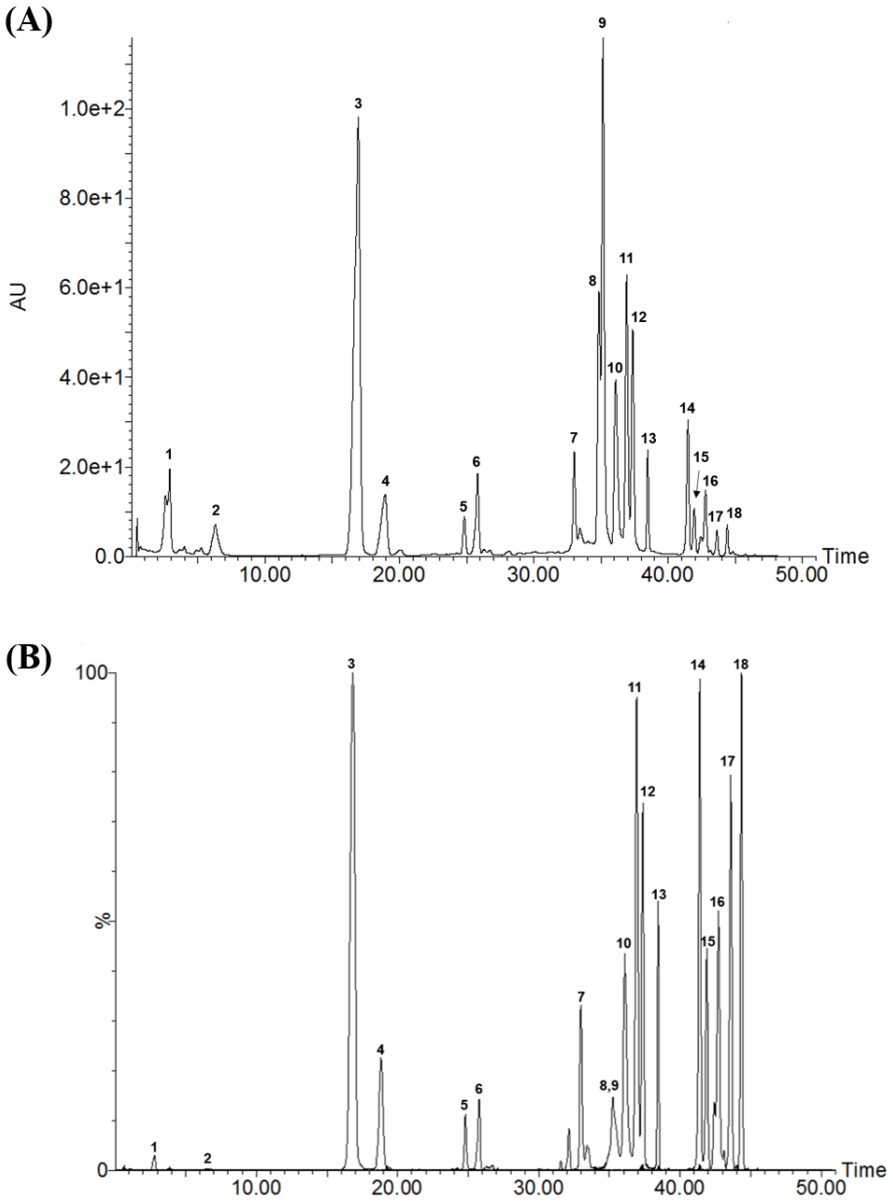

Fig. 1. UPLC-DAD (300-800 nm, full scan) (A) and UPLC-ESI-MS(+) (B) chromatograms of Rs-EtOH. Peak characterization is given in Table 1.

Table 1. Identified pigments in Rs-EtOH by UPLC-DAD-MS/MS analysis. Peak number according to Fig. 1.

Peak	**Pigment**	**RT (min)**	**Molecular formula**	**λ_{max} (nm)**	**Band III/II ratio (%)**	**Experimental *m/z* (Δ, ppm)**			**MS^2 fragments *m/z***
						$M^{\cdot+}$	**$[M+H]^+$**	**$[M+Na]^+$**	
1	Hydroxy-chlorophyll *c*$_2$	2.81	$C_{35}H_{28}O_6N_4Mg$	452, 584, 634	-	-	-	647.1743 (2.1)	625.1926, 554.1555, 549.1735
2	Chlorophyll *c*$_2$	6.47	$C_{35}H_{28}O_5N_4Mg$	452, 586, 635	-	-	609.1971 (2.8)	631.1799 (2.5)	549.1709
3	Alloxanthin	16.94	$C_{40}H_{52}O_2$	427, 451, 480	48.27	564.3970 (0.5)	-	587.3859 (1.0)	549.3735, 334.2290, 282.1976
4	Monadoxanthin	18.82	$C_{40}H_{54}O_2$	421, 445, 475	65.75	566.4122 (0.3)	-	589.4018 (0.0)	474.3481
5	Alloxanthin isomer	24.83	$C_{40}H_{52}O_2$	427, 451, 480	55.88	564.3970 (0.5)	-	587.3859 (1.0)	-
6	Alloxanthin isomer	25.82	$C_{40}H_{52}O_2$	427, 451, 480	29.00	564.3970 (0.5)	-	587.3859 (1.0)	-
7	Crocoxanthin	33.02	$C_{40}H_{54}O$	420, 444, 475	47.50	550.4179 (0.7)	-	-	535.3943, 494.3543, 458.3517, 119.0852
8	Hydroxy-chlorophyll *a*	34.72	$C_{55}H_{72}O_6N_4Mg$	421, 665	-	908.5294 (0.9)	-	-	630.2322

9	Hydroxy-chlorophyll *a* epimer	35.08	$C_{55}H_{72}O_6N_4Mg$	421, 665	-	908.5294 (0.9)	-	-	630.2322
10	Methoxylactone chlorophyll *a*	36.05	$C_{56}H_{74}O_7N_4Mg$	420, 651	-	938.5406 (0.2)	-	-	660.2441
11	Ethoxylactone chlorophyll *a*	36.93	$C_{57}H_{76}O_7N_4Mg$	421, 651	-	952.5565 (0.1)	-	-	-
12	Chlorophyll *a*	37.23	$C_{55}H_{72}O_5N_4Mg$	431, 661	-	892.5361 (0.9)	-	-	614.2377
13	Chlorophyll *a* epimer	38.48	$C_{55}H_{72}O_5N_4Mg$	412, 667	-	892.5340 (1.5)	-	-	614.2380
14	Hydroxy-pheophytin *a*	41.48	$C_{55}H_{74}O_6N_4$	407, 504, 533, 666	-	-	887.5677 (1.1)	-	609.2719
15	Hydroxy-pheophytin *a* epimer	41.95	$C_{55}H_{74}O_6N_4$	407, 504, 533, 666	-	-	887.5686 (0.1)	-	609.2719
16	β,ε-Carotene	42.78	$C_{40}H_{56}$	421, 441, 472	42.85	536.4390 (1.1)	-	-	444.3748
17	Pheophytin *a*	43.59	$C_{55}H_{74}O_5N_4$	408, 507, 538, 666	-	-	871.5743 (0.7)	-	593.2762
18	Pheophytin *a* epimer	44.34	$C_{55}H_{74}O_5N_4$	408, 507, 538, 666	-	-	871.5751 (1.6)	-	593.2766

RT: retention time.

Antiproliferative activity of Rs-EtOH

The antiproliferative activity of Rs-EtOH against A2058 cells was also evaluated. Rs-EtOH induced a concentration-dependent reduction of cell viability when compared to the control group, reaching 38.81 ± 2.70% growth inhibition at the maximum concentration tested (100 µg.ml^{-1}). The IC_{50} estimated to Rs-EtOH was > 100 µg.ml^{-1}, indicating a weak antiproliferative effect (supplementary data). However, the Rs-EtOH composition includes carotenoids unpreviously investigated for their anticancer potential, such as alloxanthin and crocoxanthin. Therefore, we fractionated Rs-EtOH in order to evaluate the antiproliferative effect of its isolated pigments.

Purification and characterization of alloxanthin and crocoxanthin

Flash liquid chromatography fractionation of Rs-EtOH (100 mg) led to the achievement of ten fractions (F1-F10), collected according to their UV absorption in a 450 nm-monitored elution (supplementary data). After UPLC-DAD-MS/MS analysis, F5 and F8 were identified as alloxanthin (**1**) (4.2 mg) and crocoxanthin (**2**) (1.2 mg), respectively. All experimental spectral data (supplementary data) were in accordance with literature (Baudelet et al., 2013; Rodriguezl, 2000; Sanz et al., 2015) and carotenoid purity grade was > 95% (UPLC-DAD chromatogram, 300-800 nm). Subsequently, we evaluated the antiproliferative activity of alloxanthin and crocoxanthin against melanoma cells.

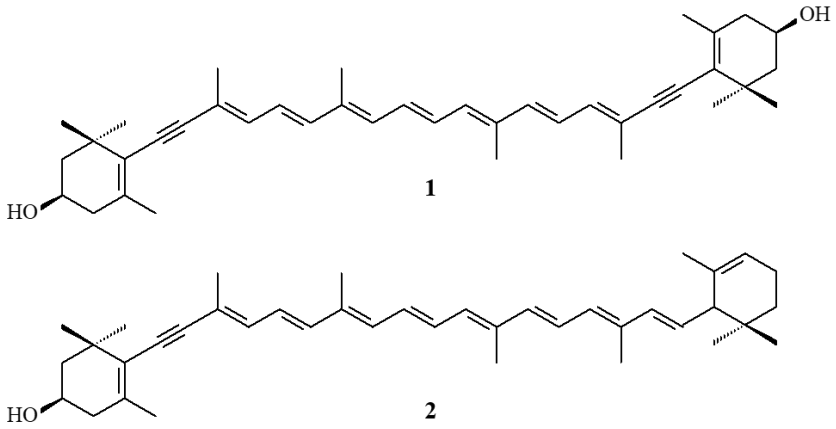

Alloxanthin and crocoxanthin inhibit proliferation of A2058 cells

Alloxanthin and crocoxanthin (1-100 µM) induced a concentration-dependent reduction in the number of A2058 cells when compared to the control group, showing IC_{50} of 29 and 50 µM, respectively (Fig. 2). Untreated cells exhibited regular epithelial morphology and became sub-confluent after 72h, indicating a high proliferation rate. In contrast, alloxanthin and

crocoxanthin (50 and 100 µM) treatments induced reduction in cell density, cell shrinkage and appearance of rounding cells (black arrows) (Fig. 2).

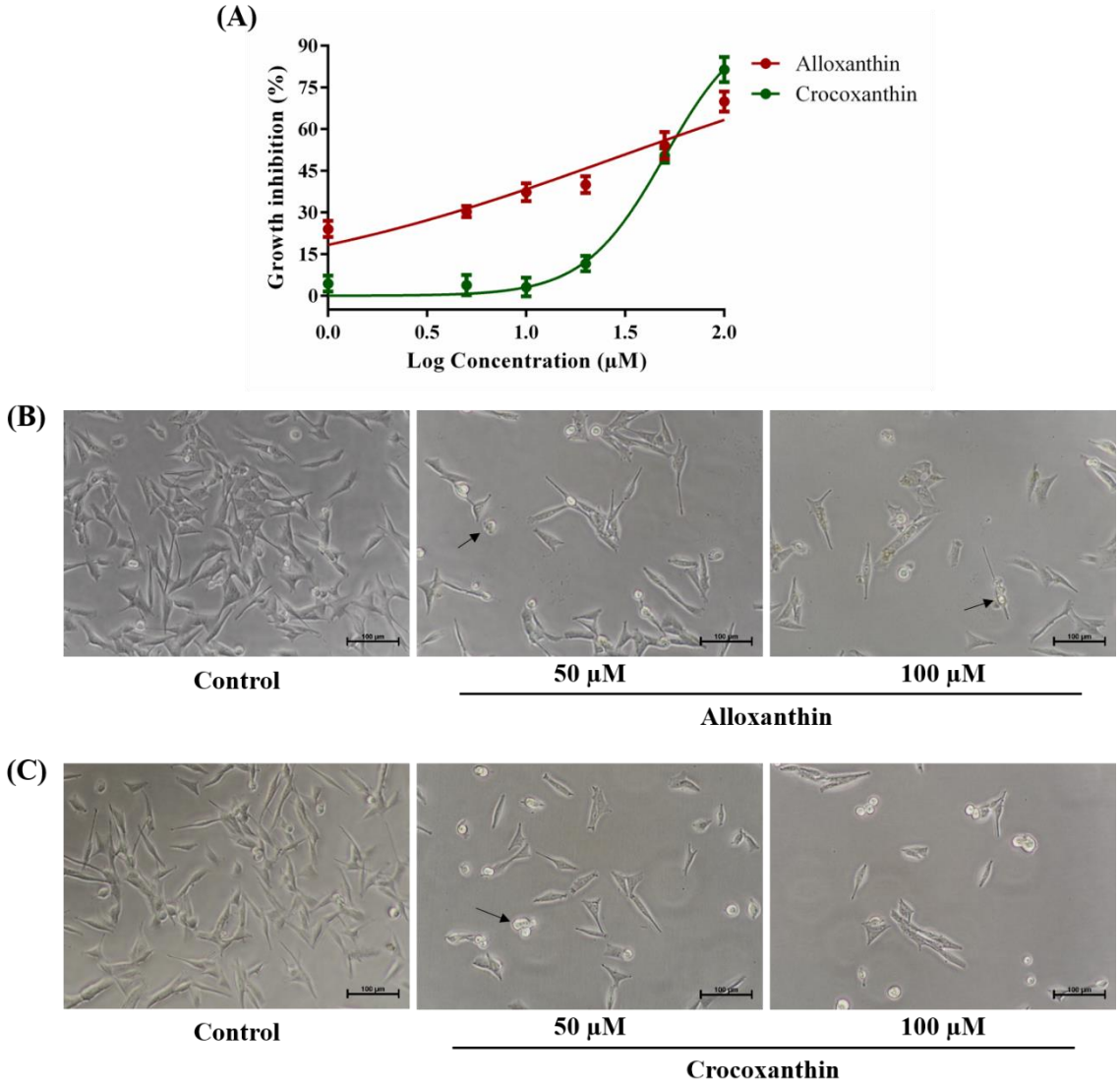

Fig. 2. Growth inhibition of A2058 cells after exposure to increasing concentrations (1-100 µM, 72h) of alloxanthin and crocoxanthin (A). Treatments with alloxanthin and crocoxanthin evoked reduction in cell density, cell shrinkage and rounding (black arrows) (B and C). Results are expressed as mean ± SEM, from at least three independent measurements (n=3).

Alloxanthin inhibits cell migration

In the cell migration assay, alloxanthin (14.5 µM, ½IC_{50}) decreased cell migration into the zone free of cells (Fig. 3) after 24h and 48h of exposure. However, crocoxanthin (25 µM, ½IC_{50}) did not significantly suppress cell migration compared to control cells.

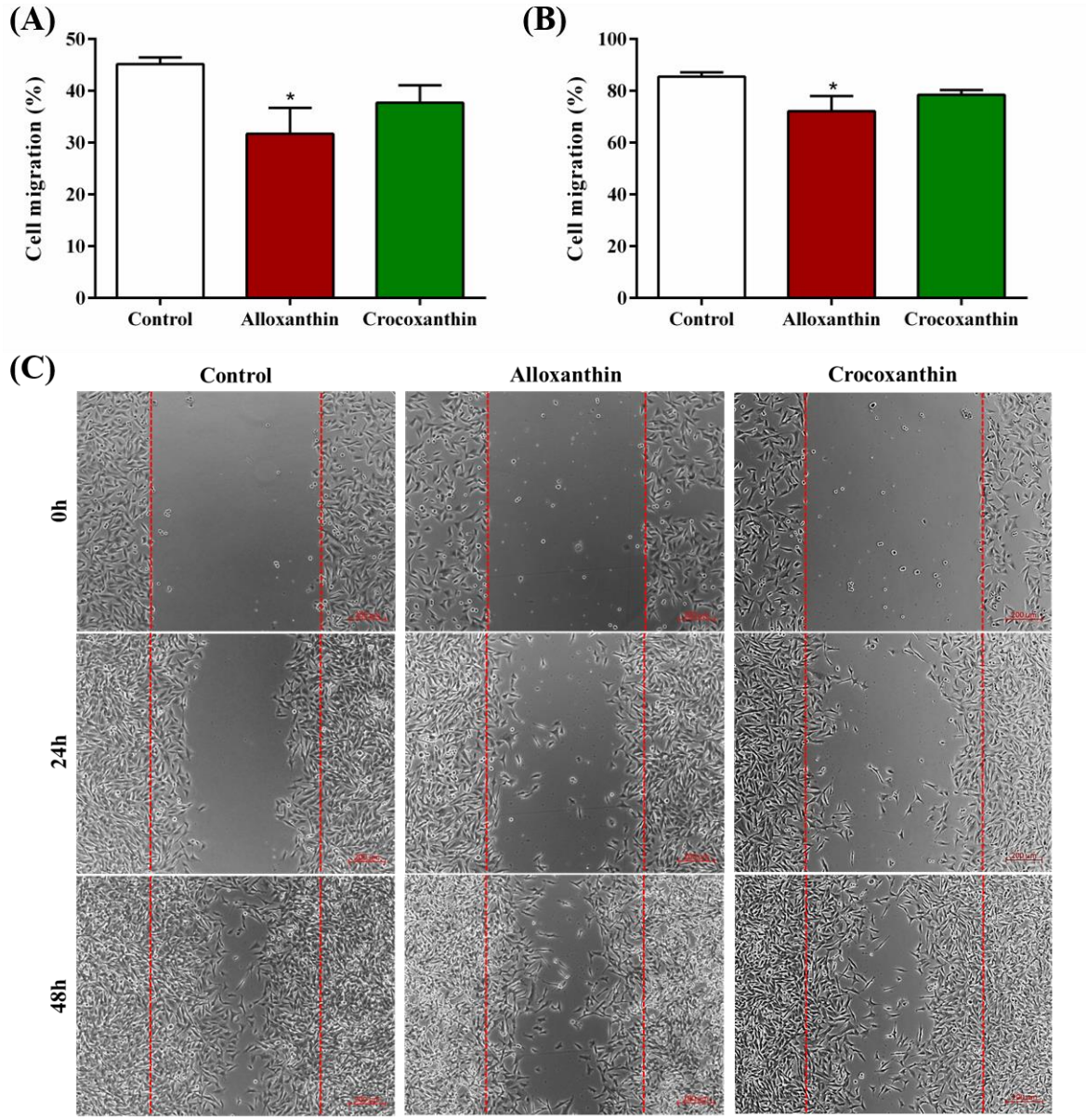

Fig. 3. Antimigratory activity of alloxanthin (14.5 µM, ½IC_{50}) and crocoxanthin (25 µM, ½IC_{50}) after 24h (A) and 48h (B) of exposure. Photomicrographs represent cell migration into the zone free of cells according to the treatment (C). Data are expressed as mean ± SEM, *p<0.05 (ANOVA one-way followed by Tukey's post-test), from at least three independent measurements (n=3).

Pro-apoptotic effect of alloxanthin and crocoxanthin

Several *in vitro* and *in vivo* studies have shown that the anticancer activity of carotenoids involves multiple mechanisms, including suppression of cell proliferation and mobility, and induction of apoptosis (Sathasivam and Ki, 2018; Sugawara et al., 2014; Wang et al., 2014). In fact, modulation of pro-apoptotic pathways is a major biochemical response promoted by

carotenoids. Typically, carotenoids up regulate the expression of important pro-apoptotic proteins (e.g. Bad, Bax, Bid, Bim), while decrease the expression of anti-apoptotic targets (e.g. Bcl-xL, Bcl-2), resulting in cell death (Juin et al., 2018; Kumar et al., 2013). In this paper, the pro-apoptotic effect of alloxanthin (29 µM, IC_{50}) and crocoxanthin (50 µM, IC_{50}) on A2058 cells was also investigated. After 72h of exposure, the number of Annexin V and 6-CFDA double-stained cells (early apoptotic cells) was expressively increased for both treatments when compared to untreated cells. In addition, alloxanthin and crocoxanthin-treated cells showed significant morphological changes, such as cell shrinkage and rounding, and tendency to form cell clumps and apoptotic bodies (Fig. 4).

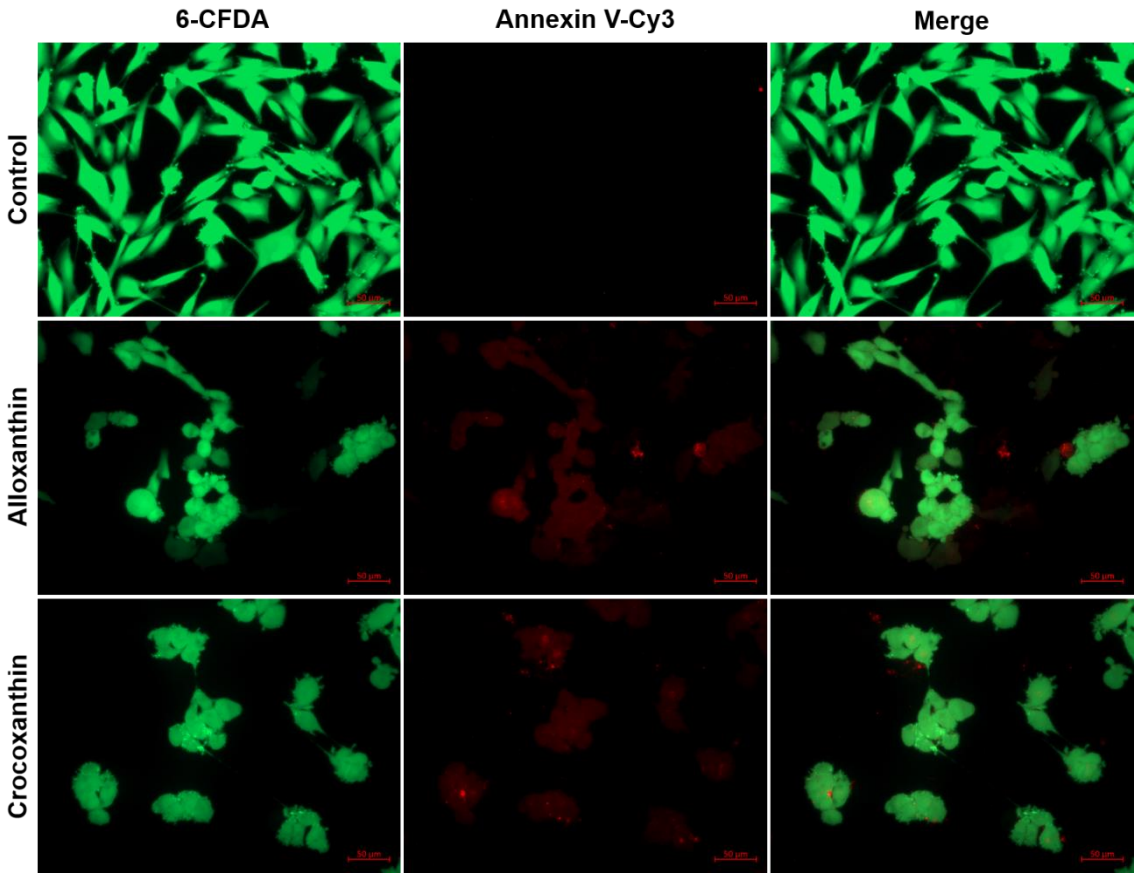

Fig. 4. Alloxanthin (29 µM, IC_{50}) and crocoxanthin (50 µM, IC_{50}) induce apoptosis in A2058 cells, after 72h of treatment. Annexin V (red) and 6-CFDA (green) double staining was observed by fluorescence microscopy. Melanoma cells in early apoptosis show both red and green stains, while cells in late apoptosis show only red stain, and untreated cells (control) are stained green only. Treated cells also presented cell shrinkage and rounding, cell clumps and apoptotic bodies formation.

Caspase-3 activation displays an important role in cell death via the intrinsic and extrinsic apoptosis pathways. Caspase-3 is a final executor caspase, responsible for apoptotic chromatin condensation and DNA fragmentation, resulting in cell dismantling and formation of apoptotic bodies (Porter and Ja, 1999). In this context, we evaluated the effect of alloxanthin (29 µM) and crocoxanthin (50 µM) on caspase-3 activity and nuclear fragmentation through enzymatic assay and DAPI staining, respectively. As shown in Fig. 5, both carotenoids induced a significant increase in caspase-3 activity after 72h of treatment. In addition, treated cells showed blebbing, DNA condensation and fragmentation (Fig. 5) compared to untreated cells, confirming the pro-apoptotic effect of alloxanthin and crocoxanthin in melanoma cells.

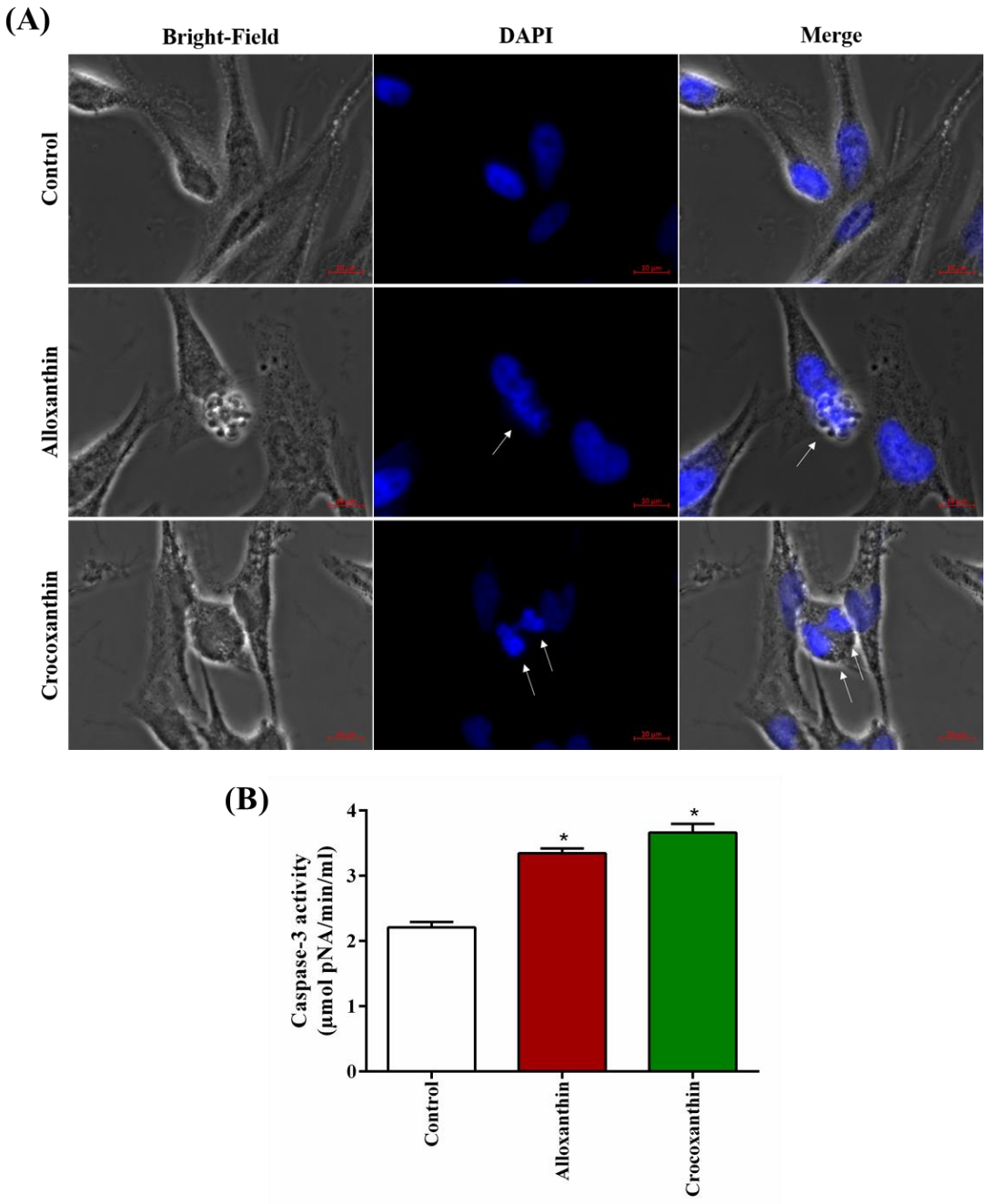

Fig. 5. Nuclear fragmentation (A) and caspase-3 activation (B) in A2058 cells exposed to alloxanthin (29 µM, IC_{50}) and crocoxanthin (50 µM, IC_{50}) during 72h of treatment. Arrows point Blebbing, DNA condensation and fragmentation after DAPI staining (A). Enzymatic activity (µmol pNA/min/ml) is expressed as mean ± SEM (B), with *p< 0.05 (*vs.* control group), according to ANOVA one-way followed by Tukey's post-test (n=3).

Alloxanthin and crocoxanthin induce accumulation of sub-G1 cells

Flow cytometry analysis revealed a significant increasing in sub-G1 cell population after exposure to alloxanthin (29 µM, IC_{50}) and crocoxanthin (50 µM, IC_{50}), characteristic of dying

cells (Fig. 6). Quantitative analysis using BD FACS Diva Software indicated 3.60 ± 0.44% of control cells were in sub-G1 phase in comparison with 6.30 ± 0.43 and 6.72 ± 0.43% of alloxanthin and crocoxanthin-treated cells, respectively (p<0.05) (Fig. 6). This result corroborates the pro-apoptotic effect observed previously for both molecules, without affecting the other cell cycle phases.

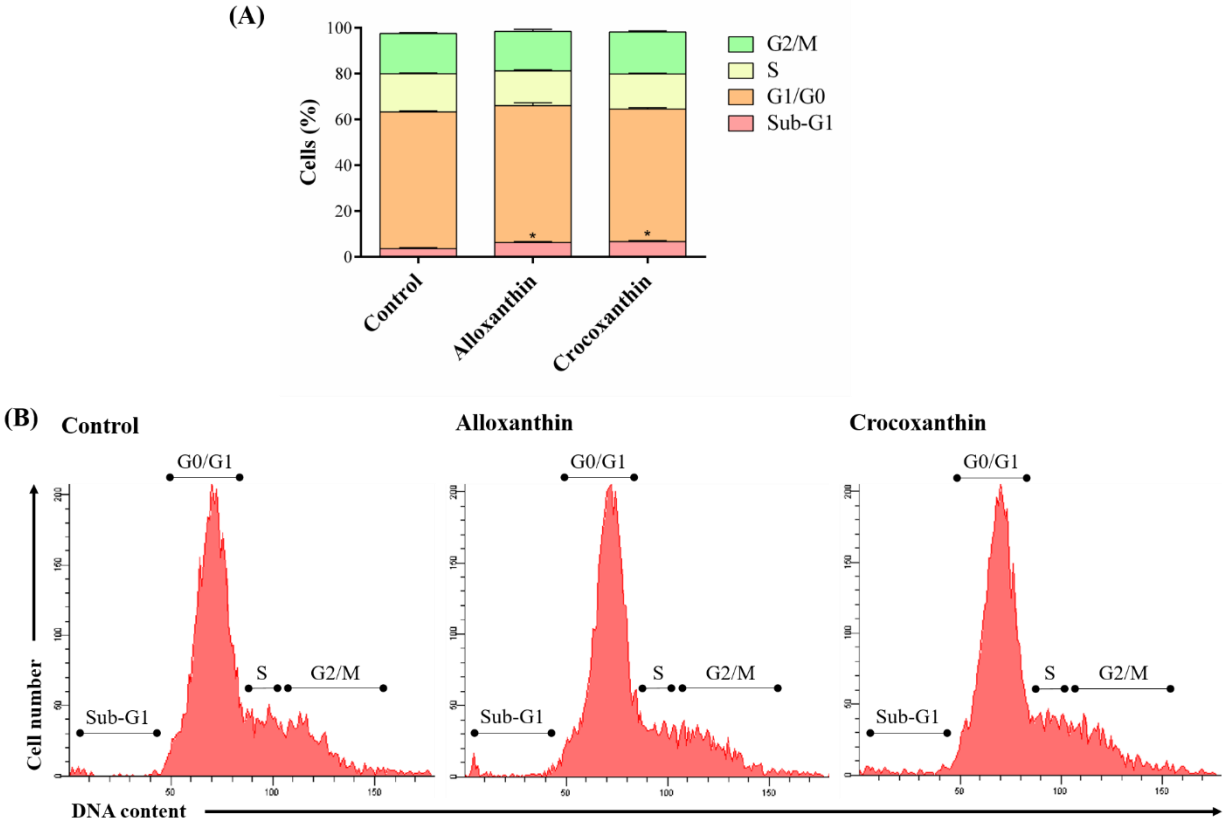

Fig. 6. Effect of alloxanthin (29 µM, IC_{50}) and crocoxanthin (50 µM, IC_{50}) on different phases of cell cycle (Sub-G1, G1/G0, S, G2/M). A2058 cells were treated for 72h, stained with propidium iodide and measured by flow cytometry, as shown in the quantitative distribution of cells in different phases of cell cycle (A) and in the representative histograms (B). Data are expressed as mean ± SEM, *p<0.05 (vs. control group) according to ANOVA one-way followed by Tukey's post-test, from at least three independent measurements (n=3).

Alloxanthin sensitizes A2058 cells to chemotherapy

Due to their metastatic and chemoresistant potential (de Oliveira Júnior et al., 2019), A2058 cells represent a good cell model to evaluate the chemosensitizing effect of cytostatic agents. They express the oncogenic BRAF V600E mutation, present in 40-70% of clinical cases (Flaherty and McArthur, 2010). Although target therapies using BRAF inhibitors (e.g.

vemurafenib) have improved the treatment of metastatic melanoma, most patients develop resistance mechanisms that limit therapeutic efficacy (Chakraborty et al., 2013; Chapman et al., 2011; Tentori et al., 2013). In this sense, we evaluated the chemosensitizing effect of *R. salina* carotenoids using the MTT assay. Alloxanthin and crocoxanthin (½IC_{50}) were combined with increasing concentrations of vemurafenib (BRAF inhibitor) or dacarbazine (alkylating agent), and tested for 72h. As shown in Fig. 7, A2058 cells were sensitive to vemurafenib (IC_{50} = 11.71 µM) but resistant to dacarbazine (IC_{50} > 100 µM). Crocoxanthin was not able to potentiate the antiproliferative activity of both anticancer drugs. However, alloxanthin enhanced the antiproliferative effect of vemurafenib by reducing its IC_{50} from 11.71 to 2.54 µM. Furthermore, alloxanthin restored the sensitivity of melanoma cells to dacarbazine (IC_{50} = 28.31 µM for combined treatment) (Table 2), reducing significantly cell density compared to monotherapy (Fig. 7).

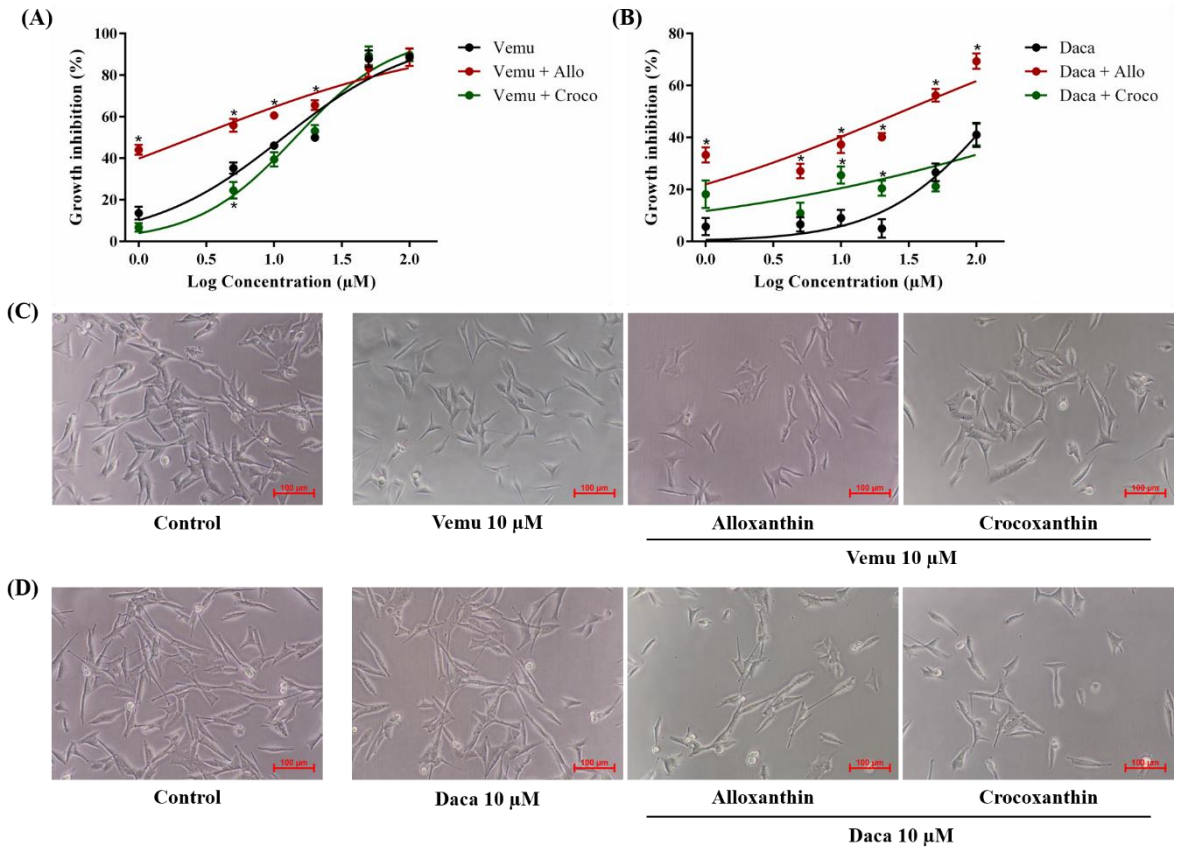

Fig. 7. Antiproliferative activity of alloxanthin (allo, 14.5 µM) and crocoxanthin (croco, 25 µM) combined to vemurafenib (vemu) (A) and dacarbazine (daca) (B) in the MTT assay. A2058 cells were grown for 72h with increasing concentrations of the anticancer drugs (1-100 µM) in the presence or absence of the carotenoids (½IC_{50}). (C) Photomicrographs show reduction of cell density promoted by combined therapies, compared to monotherapies and control groups.

Data are expressed as mean ± SEM, *p<0.05 according to unpaired Student's t test, from at least three independent measurements (n=3).

Table 2. Antiproliferative activity of monotherapies and combined therapies against A2058 cells. Data are presented as IC_{50} values and 95% confidence interval. For combined therapy, increasing concentrations of vemurafenib and dacarbazine (1-100 µM) were associated to ½IC_{50} of alloxanthin (14.5 µM) and crocoxanthin (25 µM).

Monotherapy	**IC_{50} (µM)**	**Combined therapy**	**IC_{50} (µM)**
Allo	29.16 (21.56 – 39.45)	-	-
Croco	49.92 (45.21 – 55.12)	-	-
Vemu	11.71 (10.09 – 13.58)	Vemu + Allo (½ IC_{50})	2.54 (1.76 – 3.66)
		Vemu + Croco (½ IC_{50})	14.35 (12.48 – 16.51)
Daca	>100	Daca + Allo (½ IC_{50})	28.31 (20.62 – 38.86)
		Daca + Croco (½ IC_{50})	>100

Allo (alloxanthin), croco (crocoxanthin), vemu (vemurafenib), daca (dacarbazine). IC_{50} is defined as the concentration of a compound inhibiting 50% of cell growth, calculated by non-linear regression. ½IC_{50} correspond to half of the IC_{50} value. Data are expressed as mean (95% confidence intervals), from at least three independent measurements (n=3).

In order to better characterize the sensitizing effect of alloxanthin, combination index (CI) was calculated for combined therapies (alloxanthin + vemurafenib and alloxanthin + dacarbazine) using the Chou-Talalay method (Chou and Talalay, 1984). CI values were used to check whether the antiproliferative effect was due to an additive (CI = 1), synergistic (CI < 1) or antagonistic (CI > 1) effect. As shown in Fig. 8, alloxanthin + vemurafenib combination resulted in a synergistic effect at 14.5 + 5, 14.5 + 10 and 14.5 + 50 µM treatments, while alloxanthin + dacarbazine treatment resulted in a synergistic effect at the highest concentrations (14.5 + 50 or 100 µM, respectively). In this sense, alloxanthin contributes to the antiproliferative effect of vemurafenib and dacarbazine, and may cooperate to reduce resistance in melanoma cells expressing BRAF mutation.

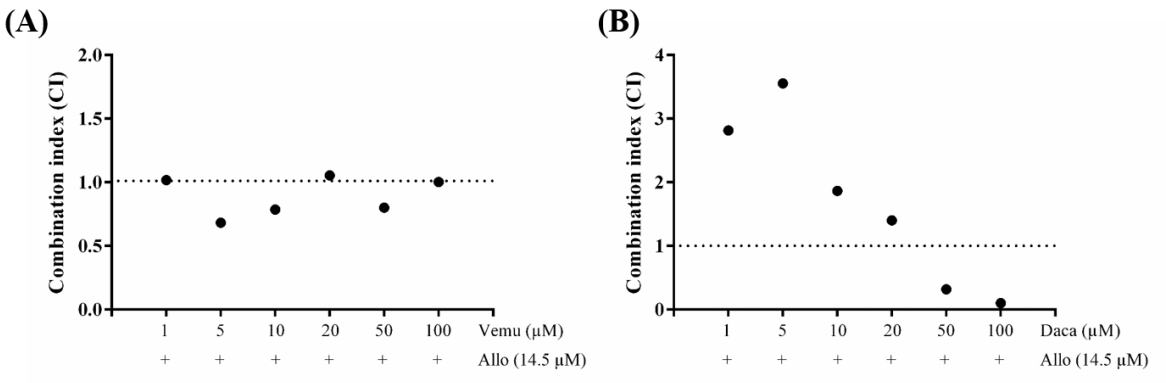

Fig. 8. Combination index (CI) for the association of alloxanthin (14.5 µM, ½IC_{50}) with vemurafenib (1-100 µM) (A) or dacarbazine (1-100 µM) (B) in the MTT assay (72h of treatment), calculated according to data shown in Table 2. CI = 1 indicates additive effect, CI < 1 indicates synergism, and CI > 1 indicates antagonism, according to Chou-Talalay method (Chou and Talalay, 1984).

4. Conclusion

This report establishes for the first time a complete pigment profile of *R. salina*, a cryptophyte microalga widely used in aquaculture and possessing an invaluable interest in the pharmaceutical and nutraceutical sectors. Alloxanthin and crocoxanthin were identified as promising antiproliferative molecules against chemoresistant melanoma cells. These carotenoids limit growth inhibition, reduce cell migration, and induce apoptosis and accumulation of sub-G1 cells. In addition, alloxanthin potentiates the antiproliferative activity of vemurafenib, a BRAF inhibitor, and restores the sensitivity of A2058 cells to dacarbazine, a conventional alkylating agent commonly used for melanoma treatment. Although further and in-depth investigations are needed, the present study demonstrates that marine carotenoids may be used as adjuvants, improving the sensitivity of melanoma cells to chemotherapy.

Acknowledgments

We thank Thierry Beignon from Synoxis Algae Company (Le Cellier, France) for the loan of LUCY photobioreactor.

Authors contributions

EN produced *R. salina* biomass; RGOJ and AB performed pigments extraction, purification and characterization by UPLC-DAD-MS/MS analysis; RGOJ, GP, LB and LP performed all pharmacological tests (cell culture, fluorescence microscopy, live cell imaging,

flow cytometry, etc.); RGOJ and NJ performed SEM analysis; RGOJ and VT participated in the design of the manuscript, data analysis and interpretation and in the writing process; LP supervised the entire study in collaboration with VT and EN.

Conflict of interest

The authors declare no conflict of interest.

Funding

This research was financially supported by the INTERREG Atlantic Area European program (Interreg EnhanceMicroAlgae project, EAPA_338/2016), and the French cancer league (Comité 17 de la Ligue Nationale contre le Cancer).

REFERENCES

Baudelet, P.H., Gagez, A.L., Bérard, J.B., Juin, C., Bridiau, N., Kaas, R., Thiéry, V., Cadoret, J.P., Picot, L., 2013. Antiproliferative activity of *Cyanophora paradoxa* pigments in melanoma, breast and lung cancer cells. Mar. Drugs 11, 4390–4406. https://doi.org/10.3390/md11114390

Casagrande, T., Cazarin, C.B.B., Roberto, M., Jr, M., Risso, É.M., Amaya-farfan, J., Grimaldi, R., Mercadante, A.Z., Jacob-lopes, E., Zepka, L.Q., 2019. Microalgae biomass intake positively modulates serum lipid profile and antioxidant status. J. Funct. Foods 58, 11–20. https://doi.org/10.1016/j.jff.2019.04.047

Chakraborty, R., Wieland, C.N., Comfere, N.I., 2013. Molecular targeted therapies in metastatic melanoma. Pharmgenomics. Pers. Med. 6, 49–56. https://doi.org/10.2147/PGPM.S44800

Chaloub, R.M., Motta, N.M.S., de Araujo, S.P., de Aguiar, P.F., da Silva, A.F., 2015. Combined effects of irradiance, temperature and nitrate concentration on phycoerythrin content in the microalga *Rhodomonas* sp. (cryptophyceae). Algal Res. 8, 89–94. https://doi.org/10.1016/j.algal.2015.01.008

Chapman, P.B., Hauschild, A., Robert, C., Haanen, J.B., Ascierto, P., Larkin, J., Dummer, R., 2011. Improved survival with vemurafenic in melanoma with BRAF V600E mutation. N Eng J Med 364, 2507–2516. https://doi.org/10.1056/NEJMoa1103782.Improved

Chou, T., Talalay, P., 1984. Quantitative dose-effect relationships: the combined effects of multiples drugs or enzyme inhibitors. Adv. Enzyme Regul. 22, 27–55. https://doi.org/10.1016/0065-2571(84)90007-4

Cisilotto, J., Sandjo, L.P., Faqueti, L.G., Fernandes, H., Joppi, D., Biavatti, M.W., Creczynski-Pasa, T.B., 2018. Cytotoxicity mechanisms in melanoma cells and UPLC-QTOF/MS2chemical characterization of two Brazilian stingless bee propolis: Uncommon presence of piperidinic alkaloids. J. Pharm. Biomed. Anal. 149, 502–511. https://doi.org/10.1016/j.jpba.2017.11.038

de Oliveira Júnior, R.G., Bonnet, A., Braconnier, E., Groult, H., Prunier, G., Beaugeard, L., Grougnet, R., da Silva Almeida, J.R.G., Ferraz, C.A.A., Picot, L., 2019. Bixin, an apocarotenoid isolated from *Bixa orellana* L., sensitizes human melanoma cells to dacarbazine-induced apoptosis through ROS-mediated cytotoxicity. Food Chem. Toxicol. 125, 549–561. https://doi.org/10.1016/j.fct.2019.02.013

de Oliveira Júnior, R.G., Christiane Adrielly, A.F., da Silva Almeida, J.R.G., Grougnet, R., Thiéry, V., Picot, L., 2018. Sensitization of tumor cells to chemotherapy by natural products: A systematic review of preclinical data and molecular mechanisms. Fitoterapia 129, 383–400. https://doi.org/10.1016/j.fitote.2018.02.025

Flaherty, K.T., McArthur, G., 2010. BRAF, a target in melanoma. Cancer 116, 4902–4913. https://doi.org/10.1002/cncr.25261

Garbe, C., Peris, K., Hauschild, A., Saiag, P., Middleton, M., Bastholt, L., Grob, J., Malvehy, J., 2016. Diagnosis and treatment of melanoma. European consensus-based interdisciplinary guideline - Update 2016. Eur. J. Cancer 63, 201–217. https://doi.org/10.1016/j.ejca.2016.05.005

Gille, A., Neumann, U., Louis, S., Bischo, S.C., Briviba, K., 2018. Microalgae as a potential source of carotenoids: Comparative results of an in vitro digestion method and a feeding experiment with C57BL/6J mice. J. Funct. Foods 49, 285–294. https://doi.org/10.1016/j.jff.2018.08.039

Habashy, N.H., Abu, M.M., Attia, W.E., Abdelgaleil, S.A.M., 2018. Chemical characterization, antioxidant and anti-inflammatory properties of Greek *Thymus vulgaris* extracts and their possible synergism with Egyptian *Chlorella vulgaris*. J. Funct. Foods 40, 317–328. https://doi.org/10.1016/j.jff.2017.11.022

Haguet, Q., Bonnet, A., Bérard, J.B., Goldberg, J., Joguet, N., Fleury, A., Thiéry, V., Picot, L., 2017. Antimelanoma activity of *Heterocapsa triquetra* pigments. Algal Res. 25, 207–215. https://doi.org/10.1016/j.algal.2017.04.034

Housman, G., Byler, S., Heerboth, S., Lapinska, K., Longacre, M., Snyder, N., Sarkar, S., 2014. Drug resistance in cancer: An overview. Cancers (Basel). 6, 1769–1792. https://doi.org/10.3390/cancers6031769

Hynninen, P.H., 1981. Mechanism of the Allomerization of Chlorophyll: Inhibition of the Allomerization by Carotenoid Pigments 1016, 1010–1016.

Jang, S., Atkins, M.B., 2014. Treatment of BRAF-mutant melanoma: The role of vemurafenib and other therapies. Clin. Pharmacol. Ther. 95, 24–31. https://doi.org/10.1038/clpt.2013.197

Juin, C., Bonnet, A., Nicolau, E., Bérard, J.B., Devillers, R., Thiéry, V., Cadoret, J.P., Picot, L., 2015. UPLC-MSE profiling of phytoplankton metabolites: Application to the identification of pigments and structural analysis of metabolites in *Porphyridium purpureum*. Mar. Drugs 13, 2541–2558. https://doi.org/10.3390/md13042541

Juin, C., Oliveira Junior, R.G. de, Fleury, A., Oudinet, C., Pytowski, L., Bérard, J.B., Nicolau, E., Thiéry, V., Lanneluc, I., Beaugeard, L., Prunier, G., Almeida, J.R.G.D.S., Picot, L., 2018. Zeaxanthin from *Porphyridium purpureum* induces apoptosis in human melanoma cells expressing the oncogenic BRAF V600E mutation and sensitizes them to the BRAF inhibitor vemurafenib. Brazilian J. Pharmacogn. 28, 457–467. https://doi.org/10.1016/j.bjp.2018.05.009

Kaňa, R., Kotabová, E., Sobotka, R., Prášil, O., 2012. Non-photochemical quenching in cryptophyte alga *Rhodomonas salina* is located in chlorophyll a/c antennae. PLoS One 7. https://doi.org/10.1371/journal.pone.0029700

Kumar, S.R., Hosokawa, M., Miyashita, K., 2013. Fucoxanthin: A Marine Carotenoid Exerting Anti-Cancer Effects by Affecting Multiple Mechanisms 5130–5147. https://doi.org/10.3390/md11125130

Lopatka, J., Malon, K., Kryk, M., 2018. Hybrid model of radio channels occupancy prediction for dynamic spectrum access. URSI 2018 - Balt. URSI Symp. 2015, 238–241. https://doi.org/10.23919/URSI.2018.8406694

Matthews, N.H., Li, W.-Q., Qureshi, A.A., Weinstock, M.A., Cho, E., 2017. Epidemiology of Melanoma, in: Cutaneous Melanoma: Etiology and Therapy. pp. 3–22. https://doi.org/10.15586/codon.cutaneousmelanoma.2017.ch1

Mosmann, T., 1983. Rapid colorimetric assay for cellular growth and survival: Application to proliferation and cytotoxicity assays. J. Immunol. Methods 65, 55–63. https://doi.org/10.1016/0022-1759(83)90303-4

Napolitano, S., Brancaccio, G., Argenziano, G., Martinelli, E., Morgillo, F., Ciardiello, F., 2018. It is finally time for adjuvant therapy in melanoma. Cancer Treat. Rev. 69, 101–111. https://doi.org/10.1016/j.ctrv.2018.06.003

Pasquet, V., Morisset, P., Ihammouine, S., Chepied, A., Aumailley, L., Berard, J.B., Serive,

B., Kaas, R., Lanneluc, I., Thiery, V., Lafferriere, M., Piot, J.M., Patrice, T., Cadoret, J.P., Picot, L., 2011. Antiproliferative activity of violaxanthin isolated from bioguided fractionation of *Dunaliella tertiolecta* extracts. Mar. Drugs 9, 819–831. https://doi.org/10.3390/md9050819

Porter, A.G., Ja, R.U., 1999. Emerging roles of caspase-3 in apoptosis. Cell Death Differ. 6, 99–104.

Prado, G., Svoboda, R.M., Rigel, D.S., 2019. What's New in Melanoma. Dermatol. Clin. 37, 159–168. https://doi.org/10.1016/j.det.2018.12.005

Rodriguezl, F., 2000. Spectral determination of chlorophylls and carotenoids.pdf 195, 29–45. https://doi.org/10.3354/meps195029

Ronca, R., Di Salle, E., Giacomini, A., Leali, D., Alessi, P., Coltrini, D., Ravelli, C., Matarazzo, S., Ribatti, D., Vermi, W., Presta, M., 2013. Long Pentraxin-3 Inhibits Epithelial-Mesenchymal Transition in Melanoma Cells. Mol. Cancer Ther. 12, 2760–2771. https://doi.org/10.1158/1535-7163.MCT-13-0487

Roos, W.P., Quiros, S., Krumm, A., Merz, S., Switzeny, O.J., Christmann, M., Loquai, C., Kaina, B., 2014. B-Raf inhibitor vemurafenib in combination with temozolomide and fotemustine in the killing response of malignant melanoma cells. Oncotarget 5. https://doi.org/10.18632/oncotarget.2610

Sanz, N., García-Blanco, A., Gavalás-Olea, A., Loures, P., Garrido, J.L., 2015. Phytoplankton pigment biomarkers: HPLC separation using a pentafluorophenyloctadecyl silica column. Methods Ecol. Evol. 6, 1199–1209. https://doi.org/10.1111/2041-210X.12406

Sathasivam, R., Ki, J.S., 2018. A review of the biological activities of microalgal carotenoids and their potential use in healthcare and cosmetic industries. Mar. Drugs 16, 1–31. https://doi.org/10.3390/md16010026

Schadendorf, D., Akkooi, A.C.J. Van, Berking, C., Griewank, K.G., Gutzmer, R., Hauschild, A., Stang, A., Roesch, A., 2018. Melanoma. Lancet 392, 971–984. https://doi.org/10.1016/S0140-6736(18)31559-9

Sengupta, S., Koley, H., Dutta, S., Bhowal, J., 2018. Hypocholesterolemic effect of *Spirulina platensis* (SP) fortified functional soy yogurts on diet-induced hypercholesterolemia. J. Funct. Foods 48, 54–64. https://doi.org/10.1016/j.jff.2018.07.007

Serive, B., Nicolau, E., Bérard, J.B., Kaas, R., Pasquet, V., Picot, L., Cadoret, J.P., 2017. Community analysis of pigment patterns from 37 microalgae strains reveals new carotenoids and porphyrins characteristic of distinct strains and taxonomic groups. PLoS One 12, 1–35. https://doi.org/10.1371/journal.pone.0171872

Spagnolo, F., Ghiorzo, P., Orgiano, L., Pastorino, L., Picasso, V., Tornari, E., Ottaviano, V., Queirolo, P., 2015. BRAF-mutant melanoma: Treatment approaches, resistance mechanisms, and diagnostic strategies. Onco. Targets. Ther. https://doi.org/10.2147/OTT.S39096

Spagnolo, F., Ghiorzo, P., Queirolo, P., 2014. Overcoming resistance to BRAF inhibition in BRAF-mutated metastatic melanoma. Oncotarget 5, 10206–21. https://doi.org/10.18632/oncotarget.2602

Sugawara, T., Ganesan, P., Li, Z., Manabe, Y., Hirata, T., 2014. Siphonaxanthin, a Green Algal Carotenoid, as a Novel Functional Compound 3660–3668. https://doi.org/10.3390/md12063660

Tentori, L., Lacal, P.M., Graziani, G., 2013. Challenging resistance mechanisms to therapies for metastatic melanoma. Trends Pharmacol. Sci. 34, 656–666. https://doi.org/10.1016/j.tips.2013.10.003

Teubner, K., Tolotti, M., Greisberger, S., Morscheid, Heike, Dokulil, M.T., Morscheid, Harald, 2003. Steady state phytoplankton in a deep pre-alpine lake: Species and pigments of epilimnetic versus metalimnetic assemblages. Hydrobiologia 502, 49–64. https://doi.org/10.1023/B:HYDR.0000004269.54705.cb

Tracey, E.H., Vij, A., 2019. Updates in Melanoma. Dermatol. Clin. 37, 73–82. https://doi.org/10.1016/j.det.2018.08.003

Tremblay, R., Cartier, S., Miner, P., Pernet, F., Quéré, C., Moal, J., Muzellec, M.L., Mazuret, M., Samain, J.F., 2007. Effect of *Rhodomonas salina* addition to a standard hatchery diet during the early ontogeny of the scallop *Pecten maximus*. Aquaculture 262, 410–418. https://doi.org/10.1016/j.aquaculture.2006.10.009

van Houcke, J., Medina, I., Maehre, H.K., Cornet, J., Cardinal, M., Linssen, J., Luten, J., 2017. The effect of algae diets (*Skeletonema costatum* and *Rhodomonas baltica*) on the biochemical composition and sensory characteristics of Pacific cupped oysters (*Crassostrea gigas*) during land-based refinement. Food Res. Int. 100, 151–160. https://doi.org/10.1016/j.foodres.2017.06.041

Vinod, B.S., Maliekal, T.T., Anto, R.J., 2013. Phytochemicals As Chemosensitizers: From Molecular Mechanism to Clinical Significance. Antioxid. Redox Signal. 18, 1307–1348. https://doi.org/10.1089/ars.2012.4573

Voskoboynik, M., Arkenau, H.T., 2014. Combination therapies for the treatment of advanced melanoma: A review of current evidence. Biochem. Res. Int. 2014. https://doi.org/10.1155/2014/307059

Vu, M.T.T., Douëtte, C., Rayner, T.A., Thoisen, C., Nielsen, S.L., Hansen, B.W., 2016. Optimization of photosynthesis, growth, and biochemical composition of the microalga Rhodomonas salina—an established diet for live feed copepods in aquaculture. J. Appl. Phycol. 28, 1485–1500. https://doi.org/10.1007/s10811-015-0722-2

Walne, P.R., 1970. Studies on food value of nineteen genera of algae to juvenile bivalves of the genera Ostrea, Crassostrea, Mercenaria and Mytilus. Fish Invest L. Ser 26, 1–62.

Wang, C., Kim, J., Kim, S., 2014. Carotenoids : New Opportunities and Future Prospects 4810–4832. https://doi.org/10.3390/md12094810

SUPPLEMENTARY DATA

Carotenoids from *Rhodomonas salina* induce apoptosis and sensitize A2058 melanoma cells to chemotherapy

Raimundo Gonçalves de Oliveira-Júnior[a], Elodie Nicolau[b], Antoine Bonnet[a], Grégoire Prunier[a], Laureen Beaugeard[a], Nicolas Joguet[c], Valérie Thiéry[a], and Laurent Picot[a*]

[a] UMRi CNRS 7266 LIENSs, La Rochelle Université, 17042 La Rochelle, France. [b] Laboratoire BRM/PBA, IFREMER, 44311 Nantes, France. [c] IDCAPS, R&D INNOV'IA, 17000 La Rochelle, France.

*Corresponding author at: UMRi CNRS 7266 LIENSs, La Rochelle Université, Curie B101 Faculté des Sciences et Technologies, Avenue Michel Crépeau, 17042 La Rochelle, France. E-mail address: laurent.picot@univ-lr.fr (Laurent Picot).

1. *Rhodomonas salina*

Rhodomonas salina CCAP 978/27 is a flagellate marine species that belongs to the Cryptophyceae class and Pyrenomonadaceae family. *R. salina* microalgae are 10-14 µm length and 5-7 µm width, with two equal flagella inserted at the apexes of the cell (Sup. Figure 1). Due to their rich levels of essential amino acids, unsaturated fatty acids and glucosides, they are commonly cultivated for use as live feed for many zooplankton species, including scallop larvae, oyster larvae and spat, and copepods. In addition, chlorophyll *a*, chlorophyll *c*, alloxanthin and β-carotene are the main pigments reported in their biochemical composition (Serive et al., 2017; Vu et al., 2016).

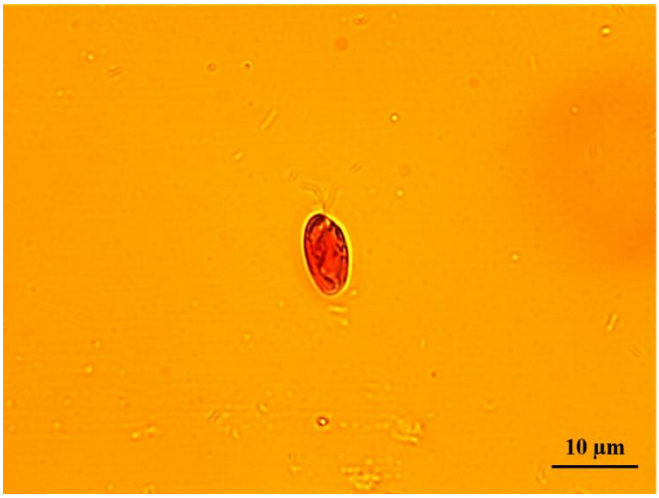

Sup. Fig. 1. *Rhodomonas salina* strain CCAP 978/27. ©IFREMER, Nantes, France.

2. Scanning electron microscopy images of *R. salina* before and after sonication-assisted extraction

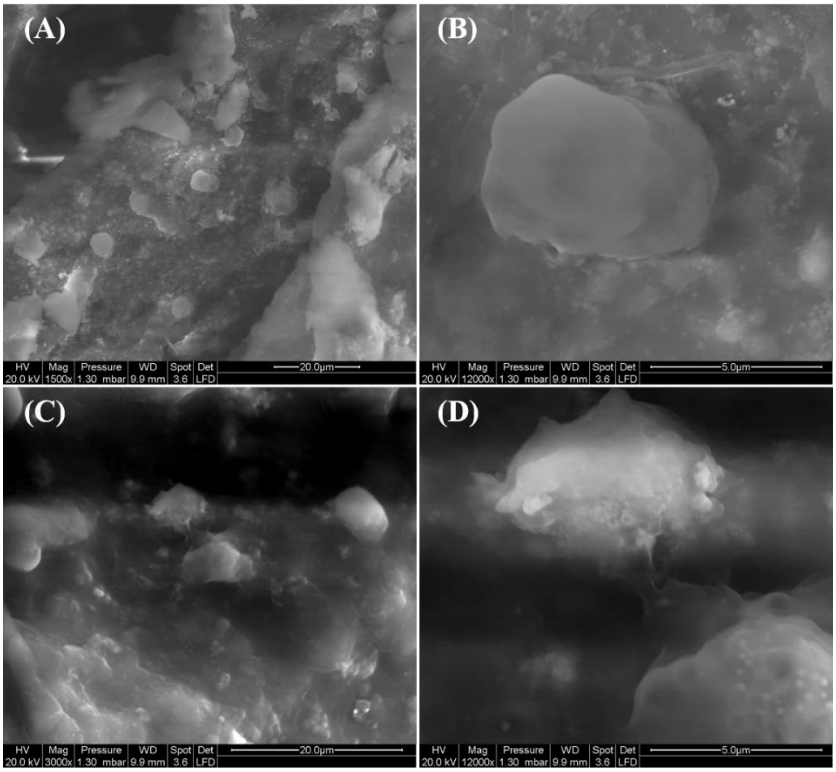

Sup. Fig. 2. Scanning electron microscopy observation of freeze-dried *R. salina* cells before (A, B) and after sonication-assisted extraction (C, D). Magnification ×3000 (A, C), ×12000 (B, D).

3. Chemical structures of the main identified pigments in *R. salina* extract (Rs-EtOH)

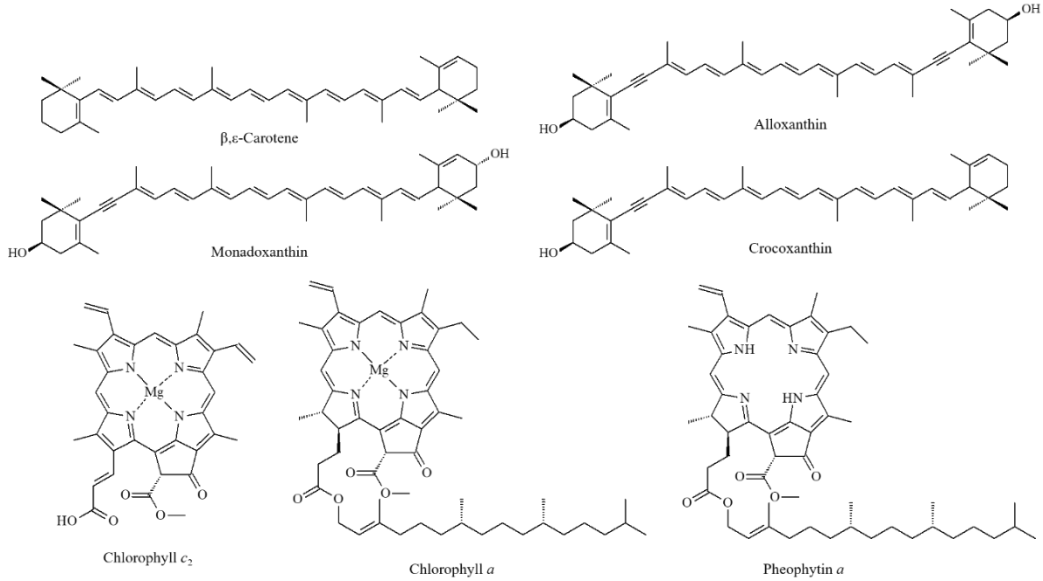

Sup. Fig. 3. Chemical structures of the main identified pigments in *R. salina* extract (Rs-EtOH)

4. Antiproliferative activity of Rs-EtOH

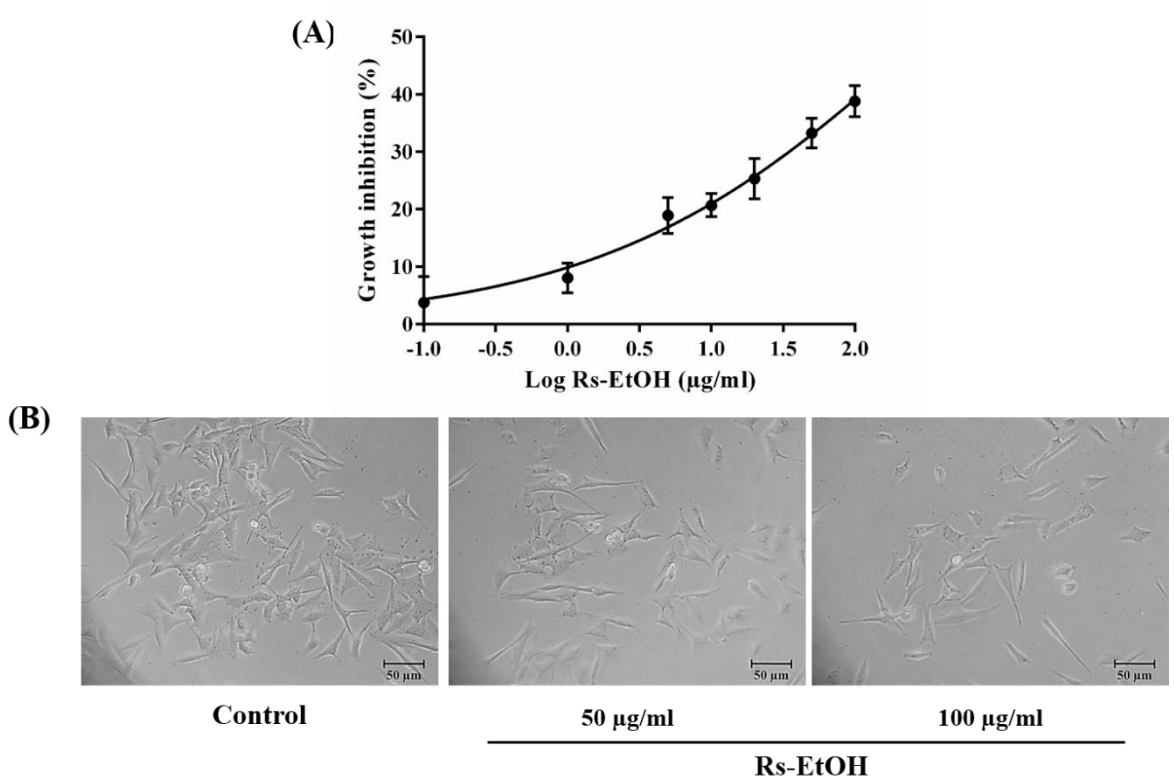

Sup. Fig. 4. Antiproliferative activity of Rs-EtOH (1-100 µg.ml^{-1}) against A2058 cells (A). Microphotographs of melanoma cells after a 72 h exposition to a control cell culture medium, or to a medium containing 50 and 100 µg.ml^{-1} Rs-EtOH (B). Results are expressed as mean ± Standard Error of the Mean (SEM), from at least three independent measurements (n=3).

5. Flash chromatography of Rs-EtOH

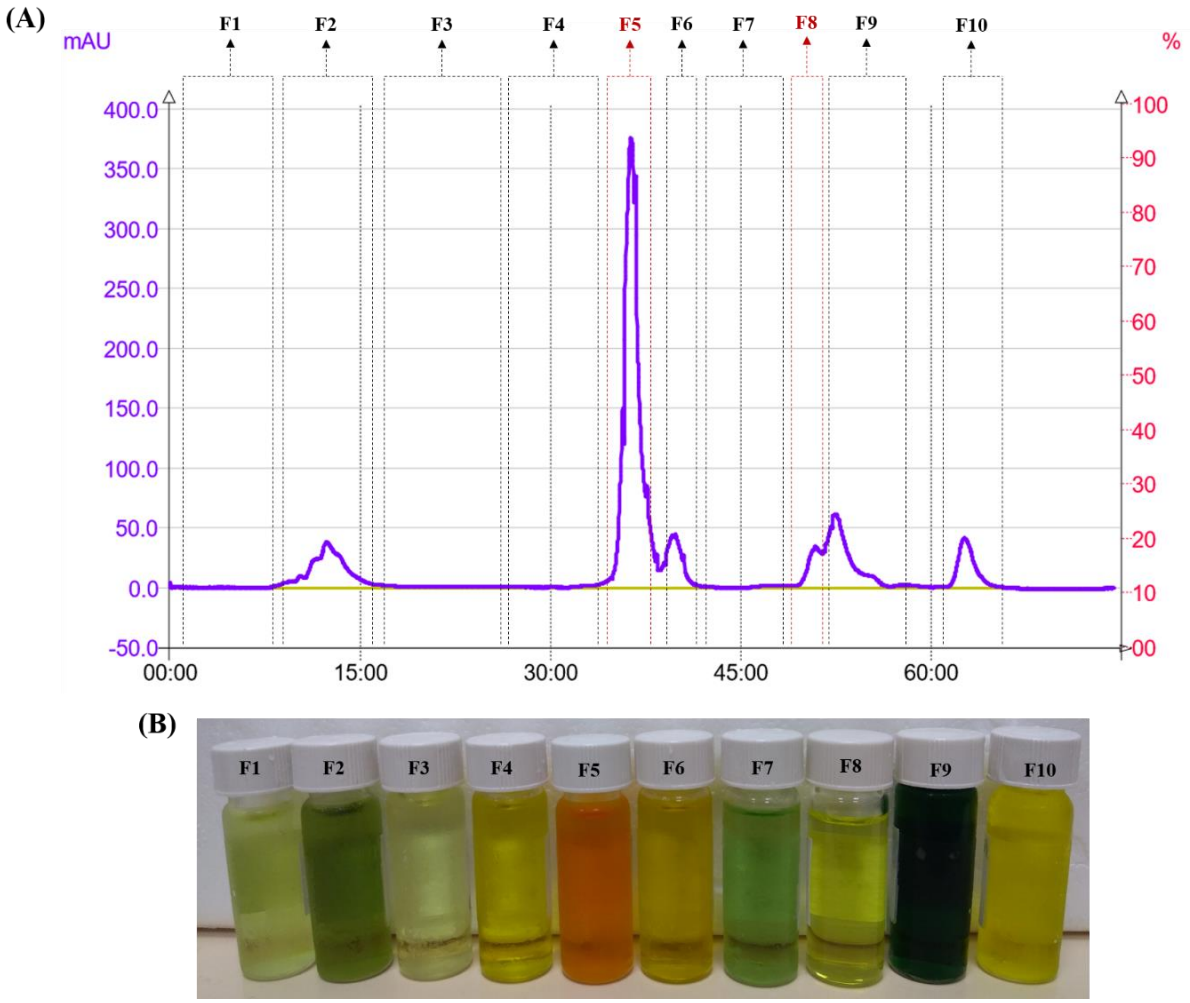

Sup. Fig. 5. Flash liquid chromatography of Rs-EtOH. Chromatogram of 450 nm-monitored elution with definition of fractions (F1-F10) collected for UPLC-DAD-MS/MS characterization and pharmacological assays (A). Fractions (F1-F10) obtained after elution (B). F5 and F8 represent alloxanthin and crocoxanthin, respectively.

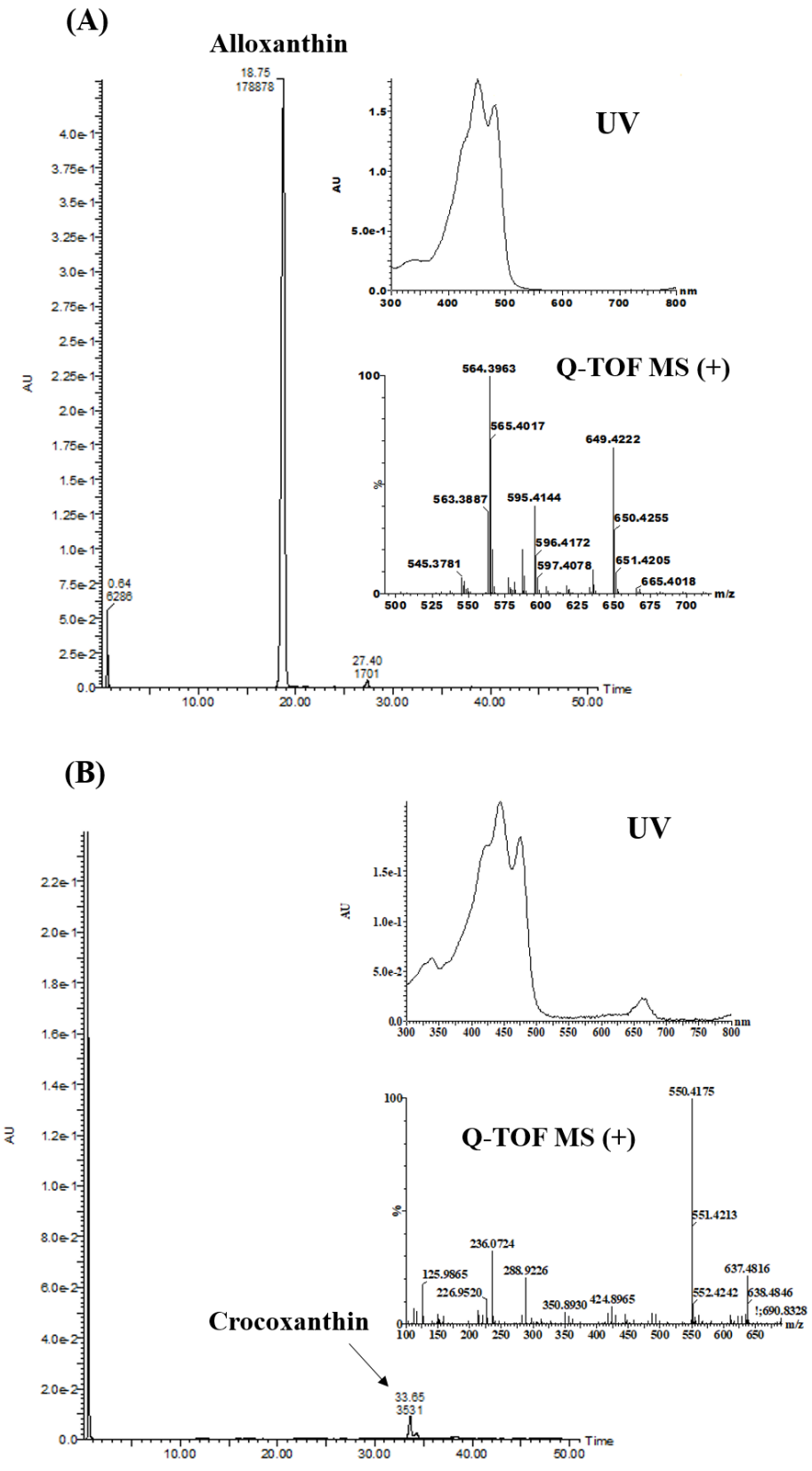

Sup. Fig. 6. UV chromatogram (450 nm), UV and Q-TOF ESI MS^+ spectra obtained for fractions F5 (A) and F8 (B), according to the flash chromatography step presented in Fig. 5.

Sup. Table 1. UPLC-DAD-MS/MS characterization of F5 (alloxanthin) and F8 (crocoxanthin), according to chromatogram presented in Figure 5.

Fraction	RT	Molecular formula	λ_{max} (nm)	Experimental m/z (Δ, ppm)			Compound
				$M^{\cdot+}$	$[M+H]^+$	$[M+Na]^+$	
F5	18.85	$C_{40}H_{52}O_2$	427, 451, 480	-	564.3963 (0.7)	587.3862 (0.5)	Alloxanthin
F8	33.65	$C_{40}H_{54}O$	420, 444, 474	550.4175 (0.2)	-	-	Crocoxanthin

RT: retention time.

Sup. References

Serive, B., Nicolau, E., Bérard, J.B., Kaas, R., Pasquet, V., Picot, L., Cadoret, J.P., 2017. Community analysis of pigment patterns from 37 microalgae strains reveals new carotenoids and porphyrins characteristic of distinct strains and taxonomic groups. PLoS One 12, 1–35. https://doi.org/10.1371/journal.pone.0171872

Vu, M.T.T., Douëtte, C., Rayner, T.A., Thoisen, C., Nielsen, S.L., Hansen, B.W., 2016. Optimization of photosynthesis, growth, and biochemical composition of the microalga *Rhodomonas salina*—an established diet for live feed copepods in aquaculture. J. Appl. Phycol. 28, 1485–1500. https://doi.org/10.1007/s10811-015-0722-2